

Research on Engineering Structures & Materials



www.jresm.org

Research Article

Numerical analysis of cracking at the nozzle junction in a distillation column

Faycal Sotehi $^{*,1}\,^{\rm a}$, Djebbara Benzerga $^{1,\rm b}$, Abdelkader Haddi $^{2,\rm c}$, Adel Chouiter $^{3,\rm d}$ Abderrahmane Belarbi $^{4,\rm e}$

¹LSCMI, University of Sciences and Technology of Oran, Mechanical Faculty, Oran, Algeria ²Univ. Artois, IMT Lille Douai, Junia, Univ. Lille, ULR 4515, Laboratoire de Génie Civil et géo Environnement (LGCgE), Béthune, France

³Institut des Sciences et des Techniques Appliquées (ISTA), University Constantine 1, Algeria ⁴LASP, University of Sciences and Technology of Oran, Mechanical Faculty, Oran, Algeria

Article Info

Article History:

Received 07 Feb 2025 Accepted 17 Oct 2025

Keywords:

Heat-affected zone; Distillation column; Composite patch repair; Cohesive zone model; Damage mechanics; ANSYS Workbench; Fatigue life

Abstract

Distillation columns are critical assets in the petrochemical industry, with nozzle-shell junctions vulnerable to fatigue damage. After 20 years of service in SONATRACH's Hassi Berkine unit, a 10 mm longitudinal crack was observed in the heat-affected zone (HAZ) of a weld. This study integrates metallurgical characterization, damage mechanics (Lemaitre model), cohesive zone modeling (CZM), and finite element analysis (ANSYS Workbench) to investigate crack initiation, propagation, and reinforcement under cyclic wind and sand abrasion loading. A local post-processor using strain history from FEM predicts damage evolution and residual life. Simulations of 63 FRP patch configurations (carbon/glass fibers, epoxy/polyurethane adhesives) reveal that a unidirectional carbon/epoxy patch (100 mm × 16 mm) optimally restores structural resistance, extending HAZ residual life by 9 service years so $\sim 46\%$. This lightweight, cost-effective composite solution is validated for in-situ repair of welded joints in petrochemical environments.

© 2025 MIM Research Group. All rights reserved.

1. Introduction

The structural integrity of distillation columns is critically important in the petrochemical industry [1]; its crucial severity was deeply clarified in [2–4], where even minor structural failures can lead to significant operational disruptions and safety hazards. Among the critical components of distillation columns is the network of nozzles, which act as the system's arteries. These nozzles facilitate the entry and exit of liquid and vapor streams at various levels while enabling the addition of reflux or treatment agents. Strategically positioned along the column, they are essential for optimizing the separation process's efficiency. However, these nozzles also represent points of structural vulnerability, apt to significant damage [5–6]. Common causes of degradation include corrosion, driven by the aggressive nature of processed substances; thermal and pressure fluctuations; mechanical stresses; and unforeseen chemical reactions [7–9]. The HAZ, a metallurgically vulnerable region adjacent to weld seams, is prone to stress corrosion cracking (SCC) and fatigue-driven damage, often leading to catastrophic failure if unmitigated [10,11]. For instance, studies by A. Takahashi et al. [12] and H. GHASSEMI-ARMAKI et al. [13] emphasize the role of microstructural embrittlement and triaxial stress states in accelerating HAZ failure, underscoring the need for robust diagnostic and repair frameworks.

*Corresponding author: favcal.sotehi@univ-usto.dz

borcid.org/0000-0003-2238-6488; dorcid.org/0009-0003-1064-1805

DOI: http://dx.doi.org/10.17515/resm2025-663me0207rs

Res. Eng. Struct. Mat. Vol. x Iss. x (xxxx) xx-xx

To address these challenges, damage mechanics has emerged as a cornerstone for quantifying structural degradation and predicting service life. The J. Lemaitre-Chaboche continuum damage model [14], validated extensively for ductile materials, enables precise simulation of damage initiation and propagation under multiaxial loading [15]. Recent advances by S. H. Mirmohammad et al. [16] and A. Bilat et al. [17] integrate damage mechanics with finite element analysis (FEA) to map crack evolution in pressure vessels, while B. A. El-Taly et al. [18] refine life-prediction methodologies for intact versus damaged structures. However, gaps persist in modeling repaired systems, particularly when composite patches are applied.

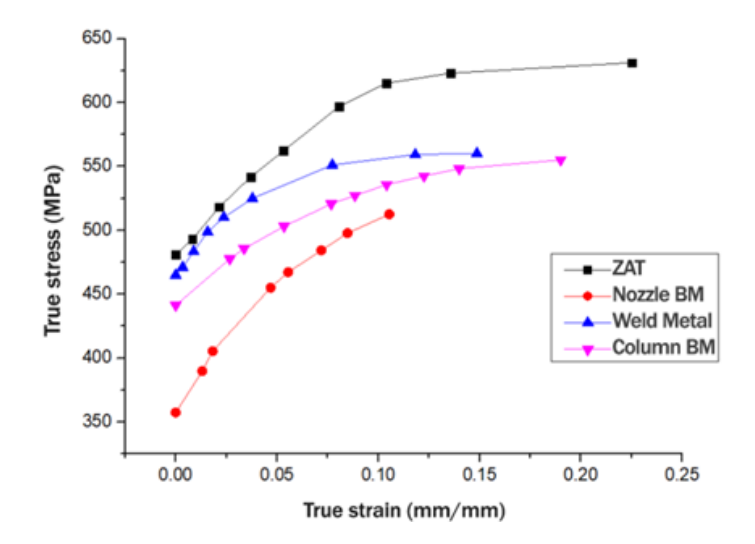


Fig. 1. Behavior law of different materials of the studied junction [19]- to be integrated in Ansys engineering data

Table 1. (a) Mechanical characteristics of the joint's materials [19]

#	Column BM	Weld Metal	HAZ (Affected SA	HAZ damage
# #	(SA 516 Grade 70)	(SMAW E7018)	516 Grade 70)	parameters [20]
Yield stress σ_y [MPa]	441.3	465	481.5	D_c = 0.22, ε_{pD} = 0%
Ultimate strength σ_u [MPa]	555.12	560	631.17	S = 2.55
Poisson's ratio	0.3	0.21	0.3	$\sigma_D = 83.5 MPa$
E [GPa]	210	180	183	$\sigma_y^\mu = 200 MPa$

Table 1. (b) Chemical characteristics of the joint's materials. [21,22]

#	C %	Cr%	Mn%	Ni%	Mo%	V%	Cu%	Al%	Si%	S%	P%	Ti%
BM	.122	.3	1- 1.7	.3	.08	.02	.3	.02	.6	.03	.03	.03
WM.	.15	.2	1.6	.3	.3	0.08	-	-	.75	.035		-

Composite patching—a rehabilitation strategy widely adopted in aerospace [23,24] but underutilized in petrochemical contexts—offers a lightweight, high-strength solution for crack arrest. Carbon fiber-reinforced polymers (CFRPs) outperform glass fibers (GFRP) in fatigue-critical applications due to superior stiffness (E1 \approx 230 GPa) and alignment adaptability, while epoxy adhesives offer enhanced thermal and mechanical durability over polyurethane [25,26], however, the PU (polyurethane) FRP reinforced beams reached a higher ultimate load [27,28]. Epoxy adhesives offer high thermal stability (Tg 50–200°C) and excellent chemical resistance, making them suitable for high-temperature petrochemical repairs. Polyurethane, with a lower Tg (-20 to

80°C), provide enhanced chemical resistance, flexibility and better vibration absorption [29]. Pioneering work by P. He et al. [30], V. Rodrigues et al. [31], D. Benzerga et al. [32] establishes cohesive zone modeling (CZM) as a gold standard for simulating adhesive debonding, yet few studies couple CZM with damage mechanics to holistically evaluate repair efficacy in HAZ scenarios. This study bridges these gaps by innovatively merging the J. Lemaitre damage criterion [33] with CZM within an Ansys Workbench FEA framework to optimize FRP-adhesive repair systems for HAZ-damaged distillation columns. By contrasting (CFRP – GFRP)/ (epoxy- polyurethane), we quantify residual life extension while resolving the competition between damage initiation and propagation at crack tip.

The present study fits into this context and relies on a real industrial case observed in the SONATRACH unit of Hassi Berkine-Algeria, where a longitudinal crack appeared at the nozzlecolumn junction after twenty years of service, under the combined effect of cyclic wind and sandy abrasion (90 km/h gusts with sand abrasion, one cycle at this speed value has been simplified to be ~2 days) induced fatigue failure in one side of the 2 mm SMAW HAZ of the junction, specifically the side exposed to the most severe wind gusts. The 2 mm thickness assumption derives from welding literature specific to low-carbon steel plate welding, particularly for vessel wall configurations. Metallurgical research on SA-516 Grade 70 steel, as documented in multiple sources [34-40], consistently confirms heat-affected zone (HAZ) widths ranging between 1.5 and 3mm. This study performs a forensic analysis of a crack discovered during a pre-commissioning inspection. The investigation focuses on wind-induced fatigue as the primary driver, justified by the crack's location and the column's idle state, which precluded operational loads. A comprehensive analysis including all operational loads is reserved for future work on in-service equipment. By integrating the Lemaitre criterion with the CZM in an ANSYS Workbench environment, we analyze the crack initiation, the evolution of damage, and the effectiveness of different composite reinforcements. A parametric evaluation of several configurations of FRP patches (type of fibers, adhesive system, dimensions) is carried out in order to identify the most efficient and economically viable solutions to extend the life of the structures.

The contribution of this work is twofold:

- propose a multiphysical framework linking the metallurgical transformations of the HAZ to mechanical performance and fatigue resistance;
- Optimize composite patch configurations capable of effectively limiting crack propagation, with validation on a real industrial case.

By resolving the competition between crack-tip damage propagation and patch-induced stress redistribution, this work provides a validated, practical framework for enhancing the structural integrity of critical petrochemical assets, offering a clear contribution to the fields of fatigue damage analysis and structural integrity management.

2 Materials and Methods

The figure 2(b) illustrates the damaged zone, in this region it located the fracture nucleated primarily at the surface of the thermally affected zone (HAZ), this crucial phenomenon, introduced particularly during welding. The HAZ surrounds the molten zone, directly influenced by the high temperatures from the fusion bead. This area undergoes significant phase transformations due to thermal cycles of heating and cooling. Temperature variations can alter the crystalline structure of the metal, leading to internal stresses [41,42].

These stresses promote the precipitation of phases, increasing the risk of surface cracks in the welded material. Particularly, surface-initiated cracks tend to propagate due to the significant damage on the external surface of the HAZ, achieving this extension (10mm) after nearly 20 years of service. The workflow, illustrated in figure 2, integrates powerful computational tools within the Ansys Workbench platform, supported by the expertise of the research team. The simulation process combines mechanical characterization, precise geometric modeling, and advanced material behavior law, along with experimental inputs to develop a locally coupled damage post-processor. The post-processor employs strain history, Figure 3(b), and crack (damage) initiation

conditions to predict damage evolution and determine the critical node (M*) residual life [43] from: intact, as well as damaged and reinforced states, figure 3 and 3(a). Figure 3 (b) demonstrates the strain history derived from a block of constant amplitude, revealing critical points of stress accumulation. This strain history directly informs the damage evolution laws applied to the HAZ material, accounting for both tensile and compressive stresses induced by bending effects.

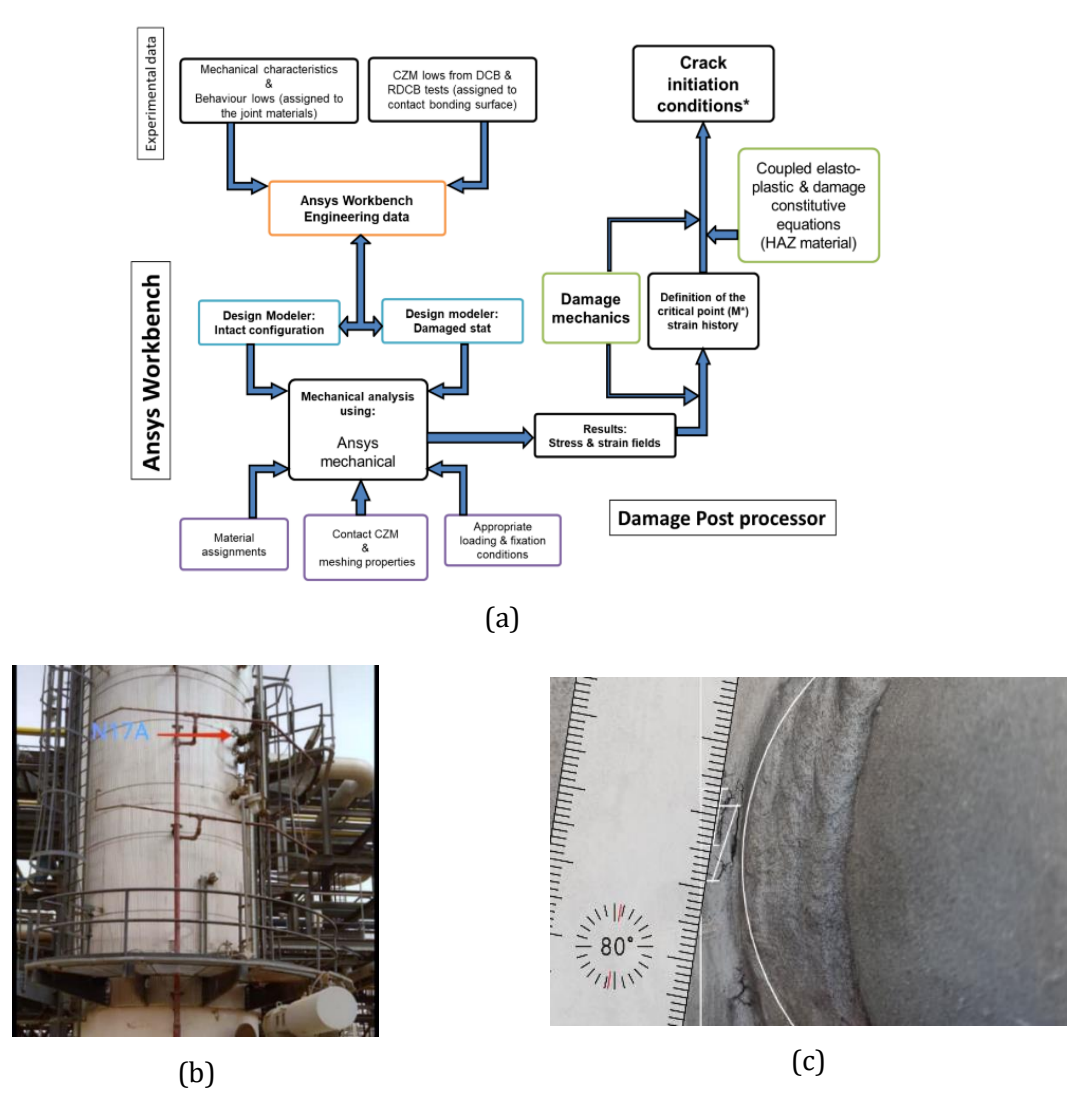


Fig. 2. (a) Damage poste-processor: Locally coupled analysis of crack initiation i.e Ansys Workbench and Damage 90, (b) Distillation column at the SONATRACH unit of Hassi Berkine-Algeria, and (c) Cracking appearance at the nozzle junction of the distillation column

The importance of the HAZ metallurgical definition [44–46] is that the strain history of the most highly stressed node, derived from the mechanical model in ANSYS Workbench, served as the foundation for evaluating the damage progression in the HAZ material, then the residual life of the global structure. Given the urgency and complexity of such scenarios, simulation-based methods are increasingly favored over purely experimental approaches. While experimental testing provides essential insights, it often requires significant infrastructure, time, and resources. By contrast, simulation allows engineers to leverage existing experimental datasets to develop highly accurate predictive models [31]. The integration of advanced computational tools, such as ANSYS Workbench, coupled with expert-developed subroutines, e.g. J. Lemaitre Constitutive Damage Criterion postprocessor, ensures rapid and precise decision-making, aligning with both time constraints and operational needs [8].

Meshing convergence results, presented in Figure 4, approve the accuracy of the simulation for both intact and damaged configurations, ensuring reliable stress field predictions. The stress

distribution, visualized in figure 5, highlights the bending effect exerted by the cantilevered nozzle on the heat-affected zone (HAZ), underlining asymmetric stress patterns and their implications for structural integrity. Pronounced tensile stresses dominate the outer surface, contrasting with compressive stresses at the inner radius amplifying bending moments at the nozzle-shell interface. The tensile-dominated outer region represents a critical zone for Mode I (opening-mode) crack initiation, as cyclic operational loads interact with the HAZ's inherent metallurgical weaknesses (e.g., grain coarsening, residual welding stresses).

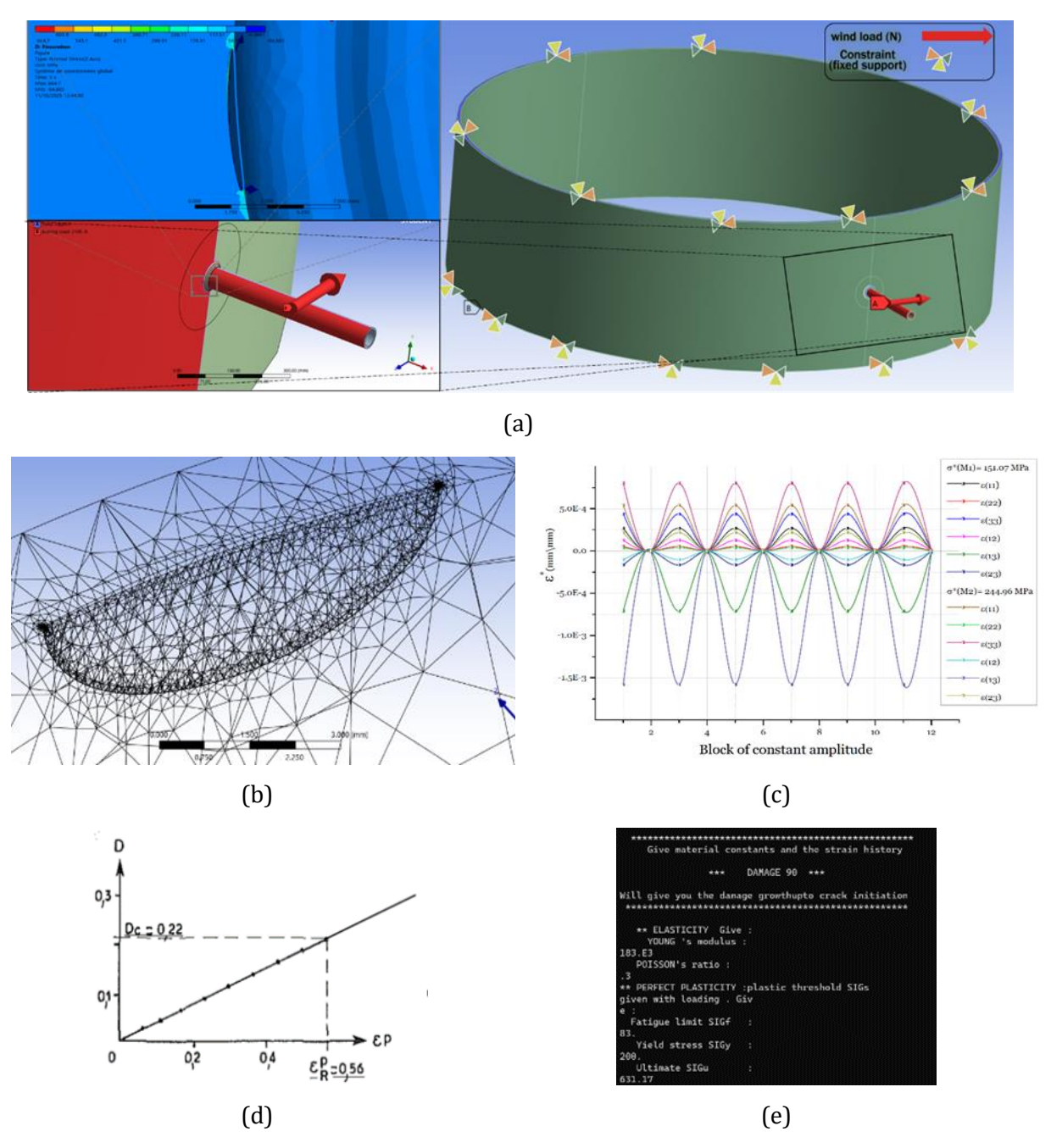


Fig. 3. (a) Model boundary conditions and support constraints with the damaged area zoomed in (b) Ansys Workbench damaged model – mesh refinement after mesh convergence (c) Strain history block of constant amplitude used to define the fatigue damage evolution, derived from intact model (d) Damage evolution low of the HAZ material (e) 'Damage90' subroutine execution with CMD in windows

Finite element analysis further reveals that strain energy preferentially accumulates on the tension side, accelerating surface-originated fatigue damage. The directional influence of wind gusts intensifies these effects, making the HAZ a primary site for structural failure in petrochemical

infrastructure. These findings were further corroborated by the detailed stress analysis in figure 6, which demonstrates the progressive increase in stress as the distance from the neutral axis to the outer surface increases. The correlation between stress levels and damage evolution is evident, with higher stresses corresponding to reduced residual life (e.g. strain history for 244.96 MPa & 151.07 MPa are illustrated in figure (3 – b) -fatigue blocks).

Unlike traditional Von Mises max stress M*(MPa) criteria [15], which are commonly employed in similar studies, this research accounted for the dominance of hoop normal stresses, a more representative metric for cantilever structures. This adaptation significantly improved the correlation between the simulation results and scientific determinations, providing a higher fidelity assessment of the structure's residual life.

The integration of experimental data with advanced simulation tools demonstrates a paradigm shift in industrial maintenance practices. This approach not only reduces reliance on time consuming experimental tests but also enhances predictive accuracy, enabling preventive interventions. The study's findings underscore the critical importance of combining simulation software proficiency, experimental datasets, and expert-developed algorithms to deliver robust and time-efficient maintenance solutions.

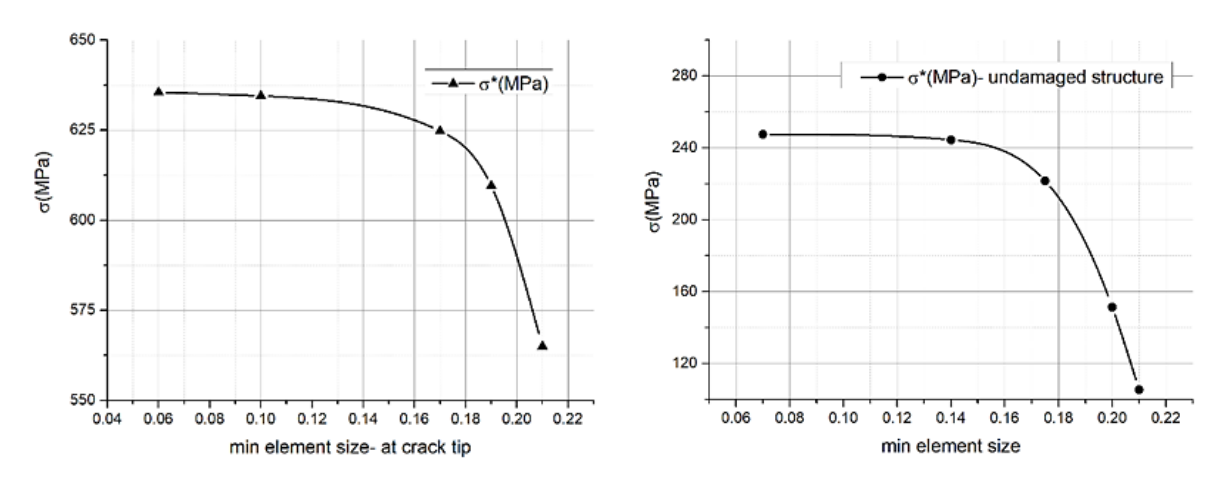
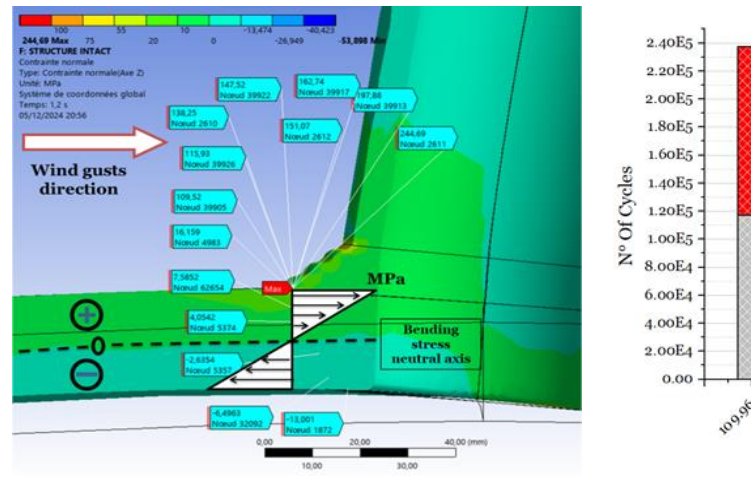
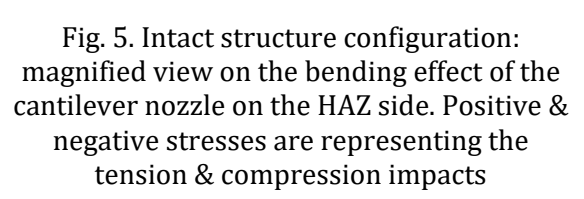


Fig. 4. Meshing convergence for the intact and damaged configurations





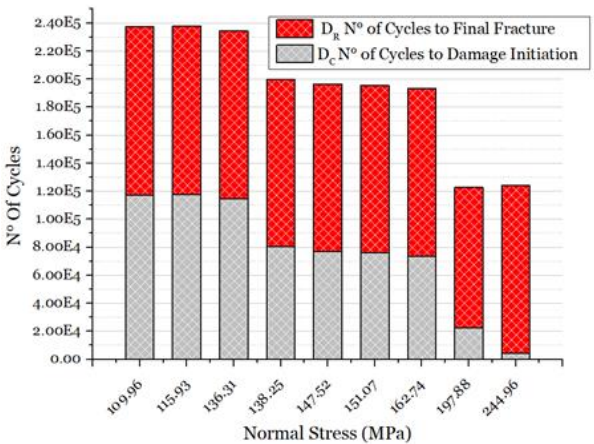


Fig. 6. Function of the distance from the neutral axis to the upper face, stress is increasing progressively while residual life decreases

In this article, we are focusing on an in-depth analysis of damage in the form of cracks that have appeared near the junction between the distillation column and the nozzle. We adopt a multiphysics approach, combining metallurgy and structural mechanics, to rigorously investigate

the emergence of cracks within the heat-affected zone located at the weld between the distillation column and the nozzle. Jean Lemaitre's damage mechanics theory [33] is a fundamental concept in the field of continuum damage mechanics. It describes the progressive deterioration of materials under external loading, leading to the eventual failure of the material. According to Lemaitre [43],, damage is quantified by a scalar damage variable D, which ranges from 0 (no damage) to 1 (complete failure). This variable represents the reduction in the effective load-bearing area of the material due to the presence of micro-defects such as voids and micro-cracks.

Equations (1) and (2) – Appendix 1, define the general kinetic damage law, with Y being the principal variable governing the damage phenomenon. Y, as shown in Equations (2) and (5), is derived as a function of effective stress ($\tilde{\sigma}$), which represents the primary driver of damage accumulation. Other constants, such as S, E, K, I, M_f , and η , reflect the material's mechanical properties, geometric parameters, and loading conditions. For simplified one-dimensional cases, the triaxiality function R_{ν} is assumed to equal 1. In three-dimensional scenarios, as described in Equation (7), R_{ν} is a function of stress triaxiality and ductility, where higher triaxiality corresponds to brittle material behavior.

The effective stress $(\tilde{\sigma})$, dependent on the geometric function f(y) (as indicated in Equation (10)), becomes a critical factor. This is particularly important in the context of cantilever configurations, where the position (y) of the stressed node relative to the neutral axis (mid-thickness of the HAZ) influences $(\tilde{\sigma})$. At the neutral axis $(y=y_0)$, stress reaches zero, while it achieves σ_{max} at the outer surfaces $(y=y_{max})$. Equations (11–19) focus on the constitutive relationships necessary to evaluate the number of cycles to failure (N_R) under low-cycle fatigue conditions. The integration of D over N cycles provides a linear correlation (Equation 17). The final expression, Equation (19), encapsulates the power-law relationship between N_R and the plastic strain rate $\Delta \varepsilon_p$, commonly referred to as the Manson-Coffin law for low-cycle fatigue. This relationship highlights the inverse proportionality between N_R and $\Delta \varepsilon_p$, emphasizing the dependence of fatigue life on plastic strain. Physically, this means that nodes experiencing higher stresses are subjected to reduced fatigue life, while nodes closer to the neutral axis $(y=y_0)$ exhibit maximum N_R due to lower stress levels [33], application results are illustrated in figure 6.

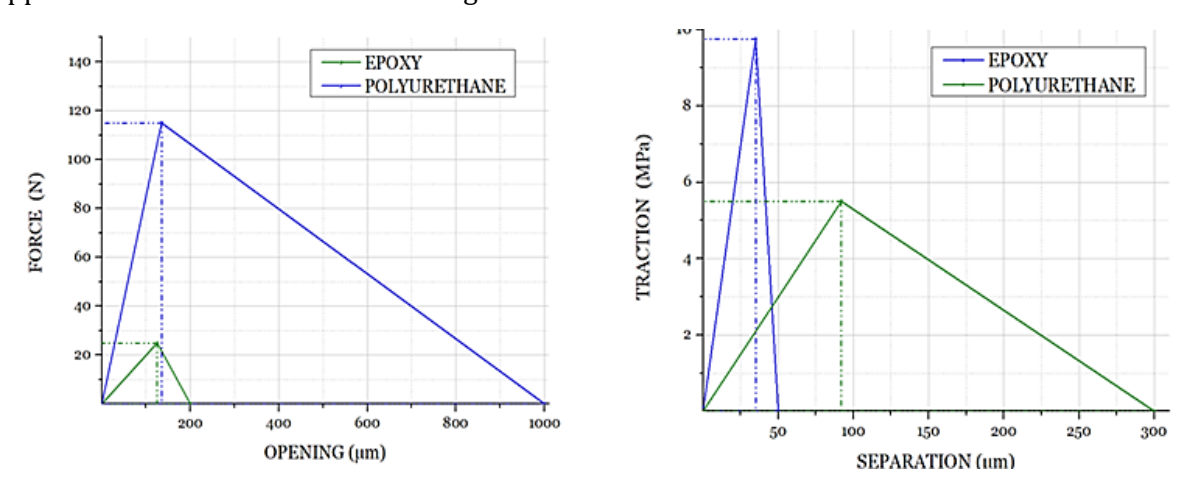


Fig. 7. Relation: Force – Opening & Traction – relative Separation of the Polyurethane & Epoxy resins, i.e. CZM, were developed from the RDCB [27]

Using the damage evolution law specific to the HAZ material, this data was experimentally set to be integrated into damage post-processor to calculate the residual life for each configuration. This approach enabled a precise assessment of structural durability under various scenarios, providing critical insights into the effectiveness of proposed reinforcement strategies and the long-term integrity of the distillation column.

The Figure 7 and Table 2 compares the RDCB (Rigid Double Cantilever Beam) derived CZMs of epoxy and polyurethane as adhesives [27], highlighting their distinct mechanical characteristics: Where epoxy exhibits higher stiffness and peak traction, indicating superior load-bearing capacity. However, its rapid softening phase limits its flexibility, making it suitable for applications

demanding high initial strength, while polyurethane demonstrates greater flexibility and an extended softening phase, which enhances energy dissipation (Gc) during crack propagation, this property makes it ideal for applications requiring adaptability to dynamic loading or deformation. By leveraging these experimentally validated CZMs [47], in finite element analysis, this study establishes a robust foundation for optimizing composite patch reinforcement bonding systems, ensuring enhanced structural performance and reliability for industrial applications [48,49].

Table 2. Strength and fracture energy of CZM adhesives [27]

#	Epoxy	Polyurethane
Temperature (°C)	22	22
Maximum Normal Contact Stress (MPa)	9.7	5.2
Contact Gap at the Completion of Debonding (mm)	0.025	0.1
Maximum Equivalent Tangential Contact Stress (MPa)	9.7	5.2
Tangential Slip at the Completion of Debonding (mm)	0.025	0.1
Artificial Damping Coefficient (s)	0.001	0.001
Power Law Exponent for Mixed-Mode Debonding	2	2

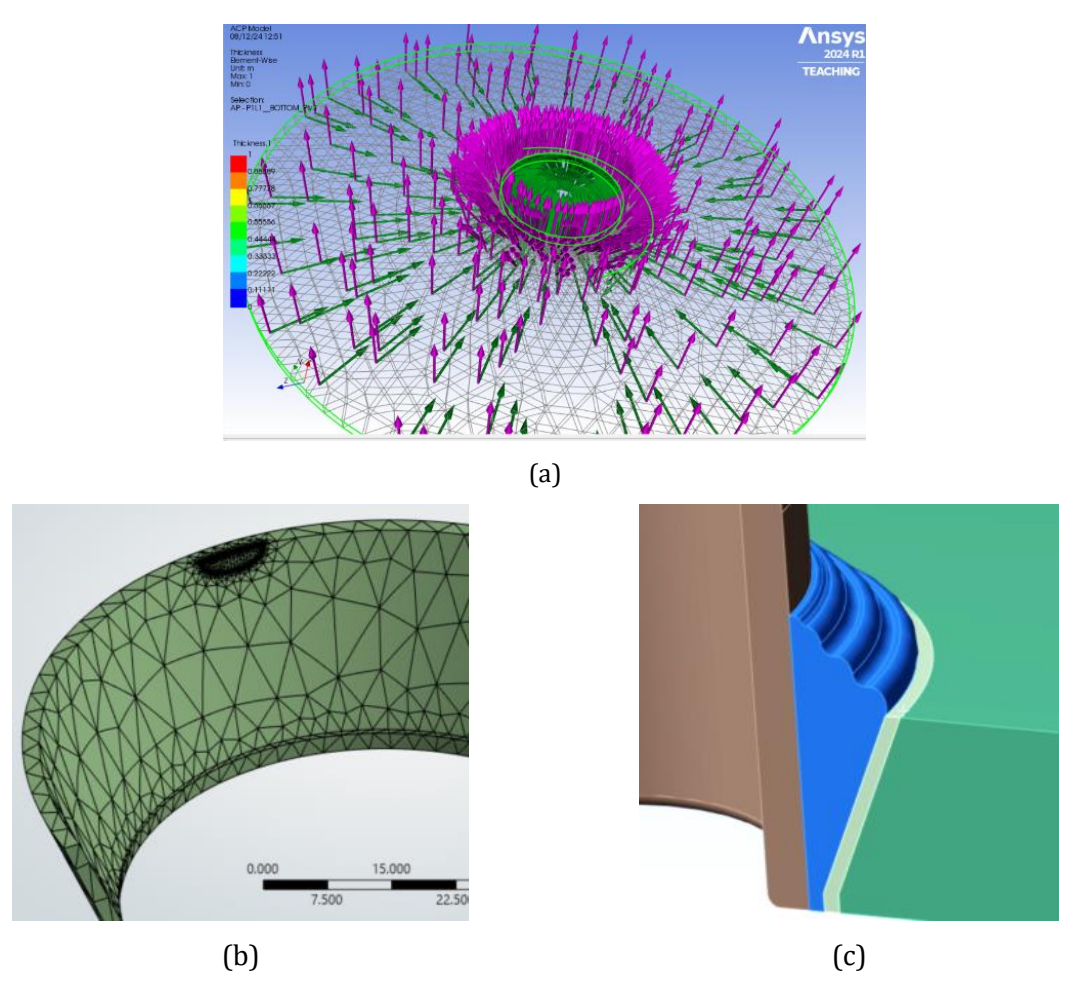


Fig. 8. (a) reinforcement patch modeling: fiber orientation (green arrows) and stacking direction (magenta), (b) Joint model (BM HAZ and WM) and (c) meshing of the damaged HAZ (with element concentration at the cracked area)

The patch dimensions reported in this study represent the optimal functional thickness required for load transfer. In a field application, this would necessitate a tapered layup at the edges to minimize peel stresses and ensure clearance. Furthermore, the model assumes optimal surface preparation (grit blasting, solvent cleaning) and curing as per adhesive manufacturer

specifications, which are critical steps for achieving the predicted performance. A detailed study of installation parameters and their optimization is a recommended topic for future workThe patch dimensions reported in this study represent the optimal functional thickness required for load transfer. In a field application, this would necessitate a tapered layup at the edges to minimize peel stresses and ensure clearance. Furthermore, the model assumes optimal surface preparation (grit blasting, solvent cleaning) and curing as per adhesive manufacturer specifications, which are critical steps for achieving the predicted performance. A detailed study of installation parameters and their optimization is a recommended topic for future work.

3. Modeling and Simulation

A 10mm crack was observed at the nozzle junction (\$\phi\$ext = 60.3mm; e = 5.54mm) of the distillation column (\$\phi\$ext = 3500mm; e = 22mm), where the mechanical properties of the welded junction (base metal - BM, weld metal - WM, heat-affected zone - HAZ) are presented in Table 1 and figure 1. Additionally, at the boundary defined by the weld bead—a circular form with a chamfered cross-section at column's liaison—lies the extremity of the heat-affected zone (HAZ). This zone takes the shape of a hollow truncated cone, characterized by a thin wall (approximately 2mm of thickness) with a height corresponding to the column wall thickness (22mm), and a predominance of the upper base, figure 8. During operation, this side-surface is subjected to a distributed bending loads transmitted by the structure, resulting in tensile stresses on the upper portion, which promote crack opening in Mode I, while moving downward, the stress gradually decreases until it reaches zero at the neutral axis, located approximately at mid-height.

Table 3. Finite Element Model Specifications

Semi-automatic mesh refinement	Number of elements	Element type	Solver version	Convergence criteria
0.1 for intact 0.14 in the damaged & repaired model	46000 43100 75000	SOLID187 (89%) CONTA174 (10%) SURF154 (1%)	Ansys Workbench 2024 R1	normal (hoop) stress stabilization function of the element size (number)

Before opening the simulation in ANSYS Mechanical, numerous studies have demonstrated the reliability and robustness of Ansys modules for simulation and validation purposes as [15,50,51]. Under the specified boundary (fixations) and loading conditions (i.e. wind load calculated using equation 20), the structure must first be meshed with respect to the meshing convergence restrictions, figure 4, for the intact structure, Table 3, a minimum tetrahedrons element size of 0.1 mm was used, resulting in approximately 46,000 elements. For damaged & reinforced configurations, a coarser mesh with a minimum element size of 1.4 mm was applied at the crack tip, leading to 43,100 for damaged structure, and 75,000 tetrahedrons elements after the application of the reinforcement, figure 3 (a). Unidirectional (UD) fibers were selected for reinforcement due to their superior performance compared to woven fibers or oriented at different angles to the direction normal to the reinforcement's circumference (indicated as 90° orientations, figure 8 (I)).

$$T = \frac{1}{2} . Cx. V^2. S. \rho \qquad So: \quad T_{max} \approx 2. kN$$
 (20)

Where;
$$Cx = 1$$
, $S_{tot} = 5.543 \ m^2$, $V_{max} = 25 \ m/s$, $\rho = 1.15 \ kg/m^3$

The wind velocity must be converted to a standardized aerodynamic loading calculation. Using the wind load equation (20), we account for air density, wind velocity, drag coefficients, and projected surface area. The stochastic nature of wind loading requires converting the variable wind conditions into a simplified constant amplitude block loading representation.

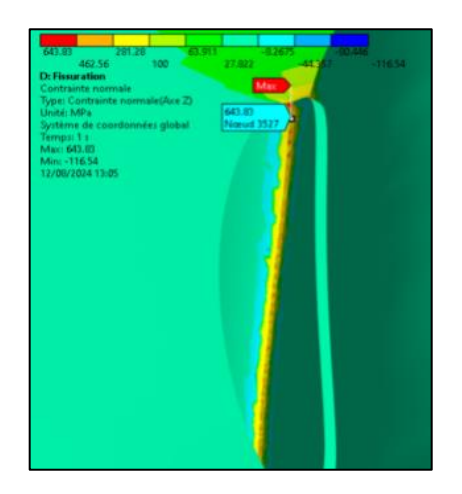
• Cycle Definition: The stress ratio is set to R = -0.01 ($\sigma_{min} = -1\% \ \sigma_{max}$) to represent the full reversal from maximum wind load to near-zero conditions.

• Life Conversion: The number of cycles to failure (N_f) is converted to years assuming one dominant load cycle every 2 days, as derived from site data: Service Life (years) = $N_f \times$ (2 days/cycle) / 365 days/year.

The simplified loading model (illustrated in Figure (3 - b)) represents the maximum stressed condition by developing a 6-component strain vector that captures the multidirectional loading effects. This approach allows for a conservative damage assessment by using the peak wind scenario as the primary loading condition. The strain vector feeds directly into the damage criterion calculation, utilizing the parameters outlined in Table 2.

4. Results and Discussion

The numerical analysis made it possible to evaluate the local constraints, the evolution of damage in the HAZ, as well as the effectiveness of composite patches. The results are presented in three steps: validation of the model, behavior of the damaged structure, then influence of the composite reinforcements.



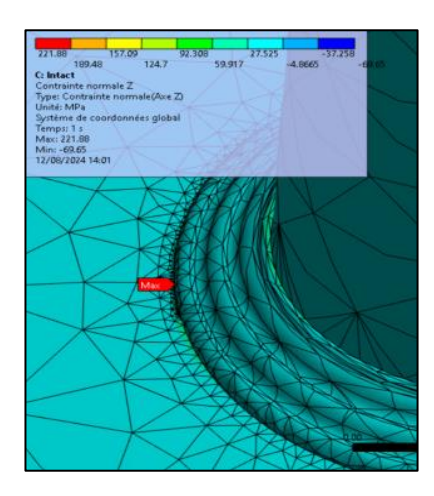


Fig. 9. Max stress results comparison: intact configuration (at the HAZ \approx 245MPa), damaged configuration (at the crack tip \approx 612.MPa)

4.1 Validation of The Numerical Model

The convergence of the mesh (Figure 4) confirmed the reliability of the calculations, both for the intact configuration and for the cracked configuration. The stress distribution (Figure 5) highlighted the effect of bending induced by the cantilever nozzle on the column wall:

- External surface of the HAZ: strong tensile stresses → critical area of initiation in mode I (opening).
- Internal surface: compression constraints \rightarrow slowing down the propagation.

Figure 9 illustrates the progressive growth of stresses as a function of distance from the neutral axis: the further away the fiber, the higher the constraint, and the longer the residual life decreases. This trend confirms that the crack initiates on the surface before spreading inwards, which is consistent with experimental observations.

4.2 Baseline Structural Performance and Damage Validation

Numerical analysis of the baseline configurations revealed critical stress concentrations confirming the observed field failure. The intact structure exhibited a maximum stress of 244.96 MPa in the HAZ region (Fig. 9). Introduction of the 10 mm longitudinal crack resulted in a severe stress concentration at the crack tip, with values reaching 612. MPa - representing a 159% increase from the intact state. This stress elevation corresponds to the observed reduction in residual life to approximately 4.9 service year (where in flawless structure = 20 years' service life).

The damage evolution pattern predicted by the Lemaitre model (via the Damage 90 post-processor) showed excellent correlation with actual field observations, with critical damage accumulation localized precisely in the wind-exposed region of the HAZ where the crack was documented.

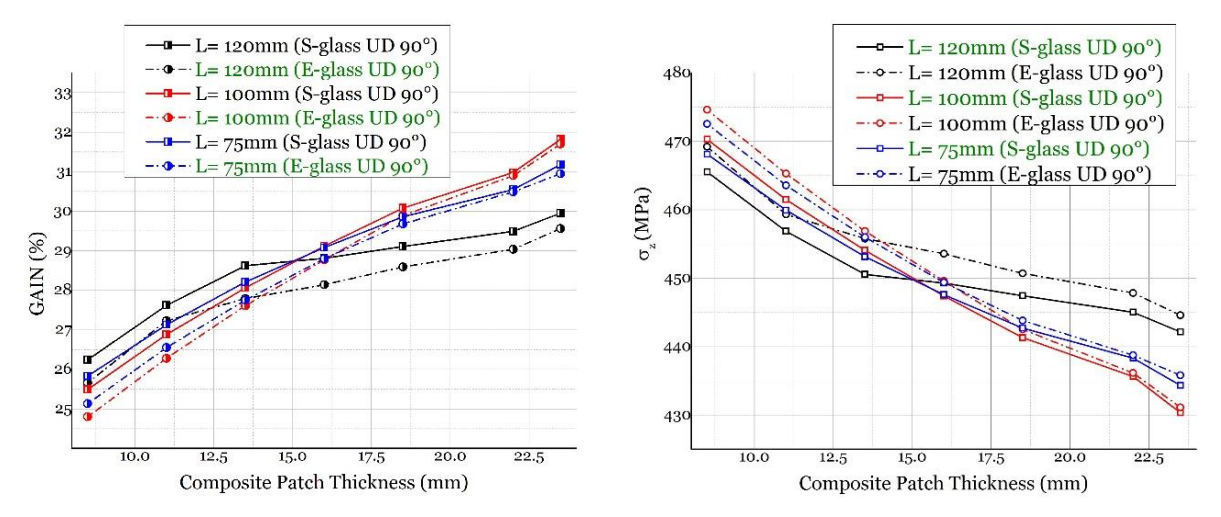


Fig. 10. The influence polyurethane CZM on glass fiber (E and S): Diminishing returns in GFRP patch effectiveness with polyurethane adhesive

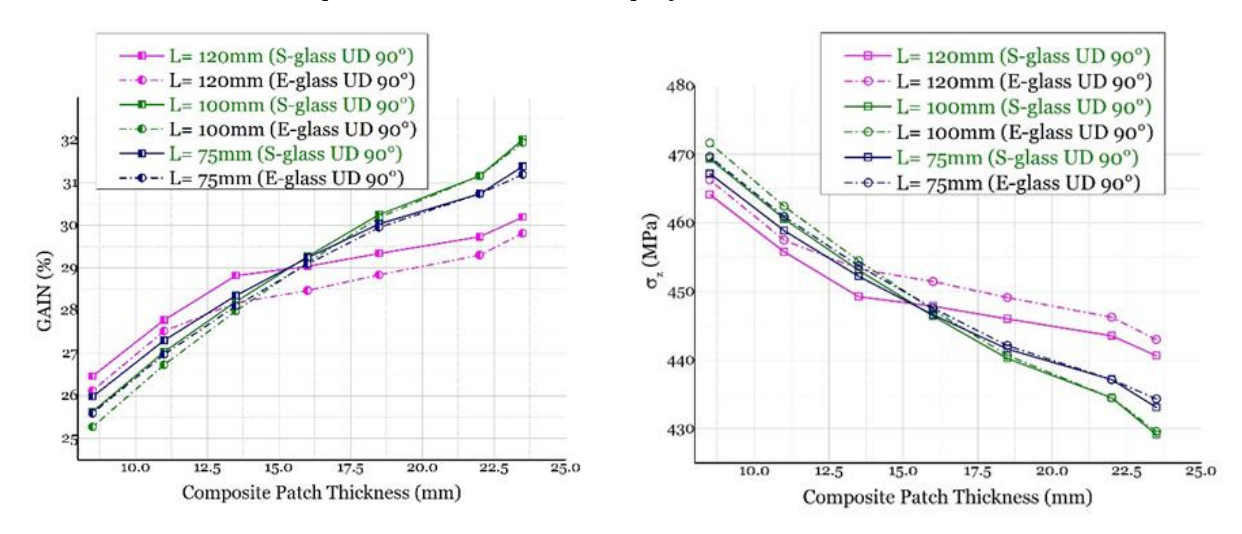


Fig. 11. Comparative stress reduction of epoxy resin for GFRP (E and S)

4.3 Parametric Analysis of Reinforcement Configurations

The comprehensive evaluation of 63 reinforcement configurations revealed systematic trends in stress reduction performance:

Figures 10-13 demonstrate the complex interplay between composite patch thickness, adhesive type, and reinforcement performance across different fiber types. For E-glass and S-glass UD 90° laminates, increasing patch thickness systematically reduced maximum stress concentration by 160-200 MPa while enhancing reinforcement efficiency by 25-32%. In carbon fiber laminates, a nonlinear relationship emerged, with epoxy adhesives outperforming polyurethane by 1.0-6.5%, attributed to the synergistic interaction between carbon's ultrahigh stiffness (230 GPa) and epoxy's rigid bonding mechanism. All patch configurations reduced stress concentrations at the crack tip, with effectiveness varying by:

- Patch material: CFRP > S-glass > E-glass (for equivalent geometries)
- Adhesive type: Epoxy > Polyurethane (across all material types)
- Geometric parameters: Longer and thicker patches performed best but with diminishing returns.

The optimal configuration - carbon/epoxy patch (100 mm \times 16 mm) - reduced maximum stress from 612. MPa to 391.4 MPa (64% reduction), effectively restoring stress levels to close intact conditions (244.96 MPa). To address the inherent uncertainties in input parameters and quantify their impact on the predicted life extension, a sensitivity analysis was conducted. This analysis focused on the two most influential variables: wind velocity Table 4, and adhesive fracture energy (Gc) -Epoxy resin against polyurethane. The carbon fiber/epoxy patch (100 mm \times 16 mm) was used as the baseline repair configuration for this assessment. The analysis reveals that the model is moderately sensitive to changes in wind velocity, as expected for a fatigue-driven process. A 20% increase in wind speed reduces the life extension by approximately 21%, underscoring the importance of using conservative, site-specific wind data for design.

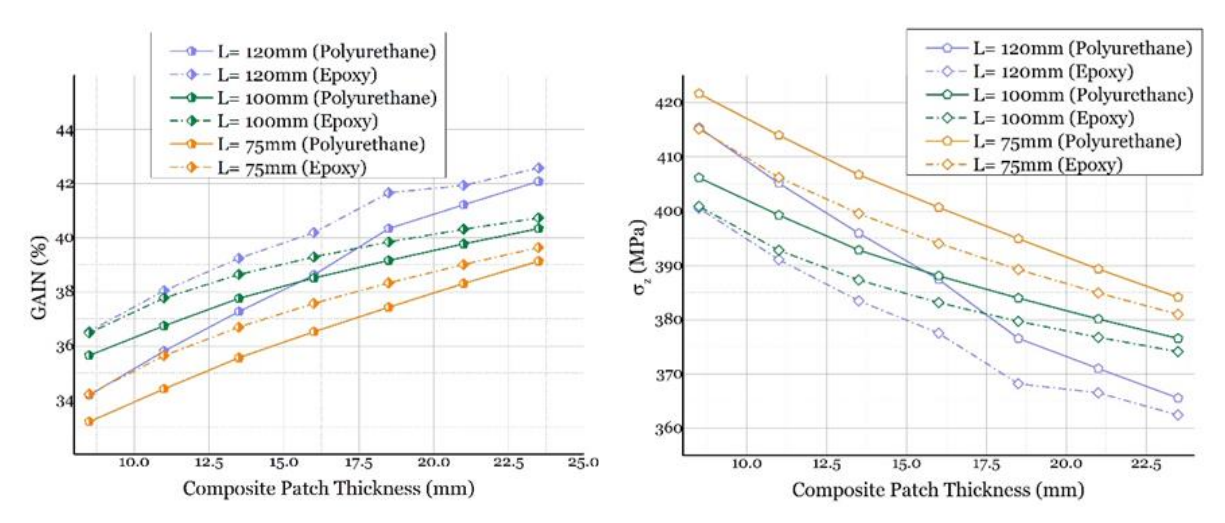


Fig. 12. Carbon fiber 230 GPa (UD 90°) reinforcement: mass-efficient restoration of structural integrity

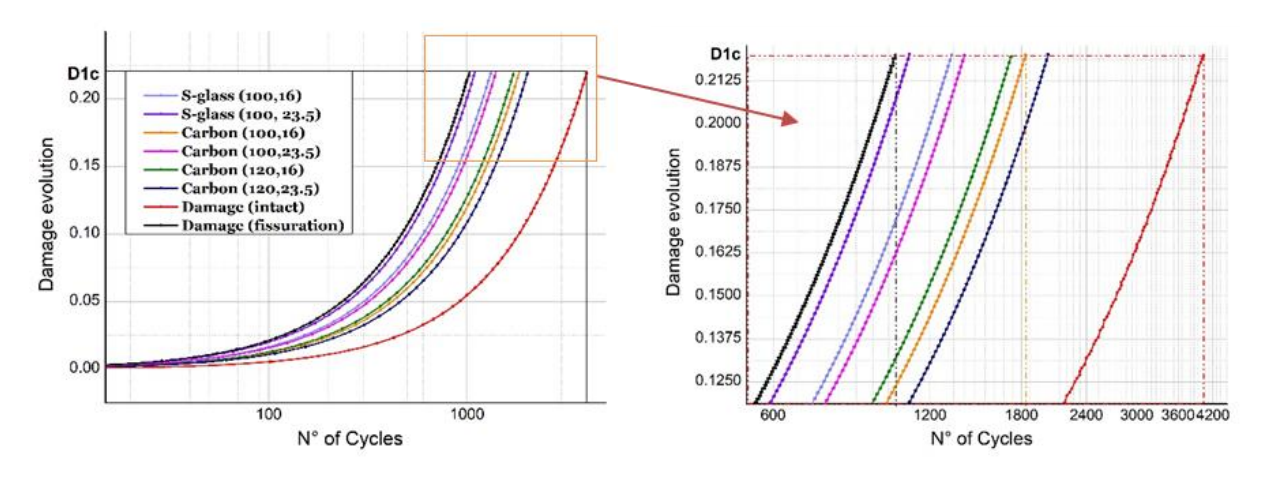


Table 4. Sensitivity analysis: ±20% of the maximum wind speed qualifying the robustness of the repairing system (CFRP 100-16): D (Damaged structure) R (Repaired)

#		σ_z (N	ЛРа)	Stress	N° of cy D		years	to Dc	Life
wind speed (m/s)	T (kN)	D	R	reduction efficiency	D	R	D	R	extension efficiency
20	1.274	476.63	237.32	50%	1630	724	8.93	39.69	198%
25	2.1	612.03	391.41	64%	893.50	1833	4.90	9.1	46%
30	2.867	828.62	535.04	65%	398	882	2.18	4.83	24%

4.4 Residual Life Enhancement

Damage evolution analysis (Fig. 13) demonstrated significant life extension across all reinforced configurations:

- Glass fiber patches: 10-30% life improvement
- Carbon fiber patches: Up to 64% life improvement
- The carbon/epoxy configuration extended residual life to approximately 2000 cycles (compared to 1030 cycles for damaged state)

4.5 Optimal Configuration Selection

Multi-criteria evaluation considering mechanical performance, mass, and cost identified the carbon fiber/epoxy patch (100 mm length \times 16 mm thickness) as the optimal solution. This configuration provided:

- Stress reduction: 64% (612. MPa $\rightarrow 391.4$ MPa)
- Life extension: 46% improvement
- Mass: 0.81 kg (compared to 1.19 kg for thicker alternatives)
- Cost-effectiveness: Best performance-to-cost ratio among all configurations

Table 5. Summary of Key Numerical Results: Comparison of the chosen configurations' residual life and additive weight

	Min N° of cycles to irreversible damage	Residual life (years)	Masse [kg]
Intact structure	4031	~20	-
Damaged structure	1030	4.9	-
Carbon-EP (100, 16)	1833	9.10	0.70
Carbon- EP (100, 23.5)	1397	7.00	1.03
Carbon-EP (120, 16)	1729	8.60	1.56
Carbon- EP (120, 23.5)	2025	10.05	2.30
S-glass- EP (100, 16)	1320	6.60	1.53
S-glass- EP (100, 23.5)	1096	5.44	2.25

5. Discussion of Mechanisms and Implications:

5.1 Mechanistic Interpretation

The superior performance of carbon fiber patches stems from their high modulus ($E_1 \approx 230$ GPa), enabling efficient load transfer and crack bridging. The epoxy adhesive's higher stiffness and strength proved more effective than polyurethane's higher fracture energy in this low-cycle fatigue application, as it ensured superior stress transfer from substrate to patch. The damage evolution curves (Fig. 13) provide particular insight: the reduced slope (dD/dN) for reinforced configurations indicates fundamentally altered damage accumulation kinetics. The optimal patch configuration effectively restored the damage progression rate to nearly intact structure behavior.

While this study provides a high-fidelity, mechanics-based assessment for an out-of-service structure, its findings are highly relevant to standards like ISO 24817 and ASME PCC-2. These standards govern the in-service repair of pressurized equipment. Our methodology offers a complementary, advanced analytical pathway that could inform future revisions of such standards, particularly for complex geometries like nozzle junctions where simplified design-by-rule methods may be overly conservative. The transition of this specific repair into active service would be managed under the framework of these standards, a process we are planning for the operational phase of this column.

5.2 Comparative Context

These findings align with aerospace composite repair studies [23,24] but advance the field through:

• Quantitative coupling of CDM and CZM methodologies

- Industrial-scale validation on petrochemical equipment
- Direct comparison of multiple material systems in identical loading conditions

The 46% life extension demonstrated has substantial practical implications, potentially adding years of safe operation and enabling planned maintenance interventions.

5.3 Limitations and Research Implications

The study's simplified constant amplitude loading represents a conservative approach but doesn't capture variable amplitude effects. Future work should address:

- Environmental degradation effects on the adhesive
- Experimental validation at full scale
- Long-term durability under operational conditions

Despite these limitations, the coupled CDM-CZM approach provides a robust framework for composite repair design that balances mechanical performance with practical implementation constraints. This comprehensive analysis demonstrates that composite patching, particularly using carbon fiber/epoxy systems, offers a technically sound and economically viable solution for extending the service life of critical petrochemical infrastructure.

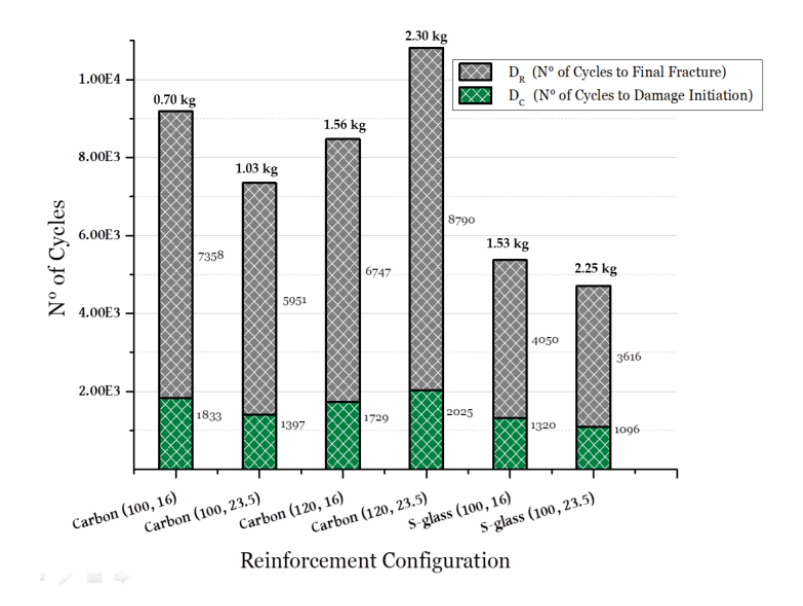


Fig.14. Damage initiation and final fracture function of patch configuration

6. Conclusions

This study focused on the analysis and strengthening of the heat affected zone (HAZ) of the nozzle-column junctions in SA 516 Grade-70 steel distillation columns, subjected to severe cyclic stresses. From a real case observed in the SONATRACH unit of Hassi Berkine (10 mm crack after 20 years of service), a multiphysics approach was developed, combining:

- Damage mechanics (Lemaitre model),
- Cohesive area modeling (CZM) for patch-substrate adhesion,
- Numerical analysis using finite element method.

The important points emerging from this study are:

- The stress analysis confirmed the critical role of hoop tensile stresses on the external face of the HAZ as the main factor for crack initiation.
- In the cracked state, the maximum stress at the crack front reaches 612. MPa, reducing the residual life of the structure of about 4.9 service units.
- The reinforcement by composite patch allows a significant improvement in mechanical strength. Among 63 configurations studied, the UD carbon-epoxy patch (100 mm 16 mm,

- 90°) showed the best performance, increasing residual life by 46% while limiting added weight (0.7 kg).
- The use of composite patches constitutes an efficient, lightweight and economical solution compared to conventional metal repairs, offering an interesting alternative for remote industrial sites.

In summary, this work proposes a robust and reproducible methodology to predict damage and design optimal composite repairs in petrochemical facilities. The developed approach constitutes a decision support tool for predictive and corrective maintenance of distillation columns.

Future research will complement this initiation-based approach by incorporating a fracture mechanics framework to model long-crack propagation, thereby enabling a full damage tolerance assessment from initial micro-damage to final failure. Further developments of this work concern:

- CZM optimization: test different cohesive laws to better represent delamination and long-term adhesion.
- Hybrid materials: explore the use of hybrid composites (carbon/glass, natural/synthetic fibers) to improve the cost-performance trade-off.
- Experimental validation: perform fatigue tests on reinforced welded samples by patch in order to confirm the digital predictions.
- Multi-scale approaches: integrate the micro structuration of the material (grains, phases) in the modeling of damage.
- Environmental assessment: study the influence of actual conditions (temperature, humidity, corrosion) on the durability of composite patches.

Nomenclature

Variable	Definition
D	Damage variable
D_c	Critical damage at crack initiation
S_D, S	Damaged sectional area (m ²), Sectional area (m ²)
Y	Strain energy density release rate
S	Damage strength material parameter
\dot{p}	Accumulated plastic strain rate
$p_{\scriptscriptstyle D}$	Damage threshold plastic strain
$R_{ u}$	Triaxiality function
N_R	Number of cycles to rupture
K	Cyclic plasticity material parameter
Μ	Strain hardening material exponent
E	Young's modulus of elasticity (GPa)
N	Poisson's ratio
$ ilde{\sigma}$	Effective stress (MPa)
σ_{eq} , σ^*	Von Mises equivalent stress (MPa) & Damage equivalent stress (MPa)
σ^D_{ij} , σ_H	Deviatoric stress tensor (MPa) & Hydrostatic stress component (MPa)
$\sigma_{\scriptscriptstyle S}$	Plastic threshold stress (MPa)
$arepsilon_{pD}$	Damage plastic strain threshold in pure tension
ρ	wind density (kg/m3)
C_X	Wind penetration coefficient
S	Exposed surface (m ²)
V	Wind velocity (m/s)

Appendix 1

By defining D as effective surface density of microdefects [14]:

$$D = \frac{\delta S_d}{\delta S} \tag{1}$$

One could start with general kinetic damage law:

$$\dot{D} = \frac{Y}{S} \cdot \dot{p} \cdot H(p - p_D) \tag{2}$$

With: Heaviside function:

$$H(x) = 0 if x < 0 , H(x) = 1 if x > 0$$
 (3)

Effective stress:

$$\tilde{\sigma} = \frac{\sigma}{(1-D)} \tag{4}$$

By the simplifications of the one-dimension condition: $R_{
u} \, = \, 1$

$$\dot{p} = \left| \dot{\varepsilon_p} \right| \tag{5}$$

$$Y = \frac{\sigma_{eq}^2 R_{\nu}}{2E(1-D)^2} = \frac{(\tilde{\sigma}^*)^2}{2E} \qquad where: \quad \tilde{\sigma}^* = \frac{\sigma_{eq} R_{\nu}^{1/2}}{(1-D)}$$
 (6)

And: (in general three-dimensional case)

$$\sigma_{eq} = \sqrt{\frac{2}{3} \cdot \sigma_{ij}^D \cdot \sigma_{ij}^D} \tag{7}$$

$$R_{\nu} = \frac{2}{3} \cdot (1 + \nu) + 3 \cdot (1 - 2\nu) \cdot \left(\frac{\sigma_H}{\sigma_{eq}}\right)^2$$
 (8)

$$\sigma_{ij}^{D} = \sigma_{ij} - \sigma_{H} \cdot \delta_{ij} \quad Or: \quad \sigma_{H} = \frac{1}{3} \sigma_{kk}$$
(9)

So:
$$\dot{D} = \frac{\sigma^{*2}}{2ES(1-D)^2} \cdot |\dot{\varepsilon_p}| \quad if: \varepsilon_p > p_D$$
 (10)

From Ramberg Osgood hardening low coupled with damage:

$$\varepsilon_p = \left(\frac{\tilde{\sigma}_{eq}}{K}\right)^{\eta}; \quad \text{Or:} \quad \tilde{\sigma}_{eq} = K. \left(\varepsilon_p\right)^M \quad \text{and:} \quad \eta = \frac{1}{M} \quad (11)$$

For one-dimensional case:

$$\dot{\varepsilon}_p = \frac{\eta}{K} \left(\frac{\tilde{\sigma}}{K} \right)^{\eta - 1} . \dot{\tilde{\sigma}} \tag{12}$$

Bending stress for cantilever condition:

$$\dot{\varepsilon}_p = \frac{\eta}{K} \left(\frac{\frac{M_f}{I} \cdot f(y)}{K} \right)^{\eta - 1} \cdot \dot{\tilde{\sigma}} \tag{13}$$

The accumulated plastic strain after one cycle:

$$\frac{\delta p}{\delta N} = \int_{1 \text{ cycle}} |\dot{\varepsilon}_p| \ dt = 2\Delta \varepsilon_p \tag{14}$$

And for N cycle:

$$p_{(N)} = 2N\Delta.\,\varepsilon_p \tag{15}$$

After mathematical model simplification, damage is evaluated for one cycle as:

$$\frac{\delta D}{\delta N} = \int_{1 \text{ cycle}} \dot{D} dt = \frac{\sigma_s^2}{4ES(1-D)^2} \cdot \Delta \varepsilon_p$$
 (16)

$$\frac{\delta D}{\delta N} = \frac{(\Delta \tilde{\sigma})^2}{4FS} \cdot \Delta \varepsilon_p \tag{17}$$

So:

$$\frac{\delta D}{\delta N} = \frac{\left(K(\Delta \varepsilon_p)^{\eta}\right)^2}{4ES} \cdot \Delta \varepsilon_p$$

$$\frac{\delta D}{\delta N} = \frac{K^2}{4ES} \cdot \left(\Delta \varepsilon_p\right)^{1+2\eta}$$
(19)

$$\frac{\delta D}{\delta N} = \frac{K^2}{4ES} \cdot \left(\Delta \varepsilon_p\right)^{1+2\eta} \tag{19}$$

For N cycles, counting on $\Delta \varepsilon_p$ being constant with the linear relation between N and D:

$$D = \int_{1 \text{ cycle}} \frac{\delta D}{\delta N} \, \delta N = \frac{K^2}{4ES} \cdot \left(\Delta \varepsilon_p \right)^{1+2\eta} (N - N_0) \tag{20}$$

Where:

$$N_0 = \frac{p_D}{2\Delta\varepsilon_p} \tag{21}$$

The number of cycles to failure is reached when $D = D_c$:

$$D_c = \frac{K^2}{4ES} \cdot \left(\Delta \varepsilon_p\right)^{1+2\eta} \left(N_R - \frac{p_D}{2\Delta \varepsilon_p}\right) \tag{22}$$

Finally:

$$N_R = \frac{p_D}{2\Delta\varepsilon_p} + \frac{4ESD_c}{K^2} \cdot \left(\Delta\varepsilon_p\right)^{-(1+2\eta)} \tag{23}$$

References

- [1] Hosseini SMS, Shahanaghi K, Shasfand S. Functional model of integrated maintenance in petrochemical industries. Int J Eng Trans C Asp. 2024;37(6):1106-17. https://doi.org/10.5829/IJE.2024.37.06C.07
- [2] Nakaiwa M, Huang K, Endo A, Ohmori T, Akiya T, Takamatsu T. Internally heat-integrated distillation columns: Α review. Chem Des. 2003;81(1):162-77. https://doi.org/10.1205/026387603321158320
- AK. Heat integrated distillation operation. Appl Energy. 2010;87(5):1477-94. https://doi.org/10.1016/j.apenergy.2009.10.014
- [4] Skogestad S, Morari M. Understanding the dynamic behavior of distillation columns. Ind Eng Chem Res. 1988;27(10):1848-62. https://doi.org/10.1021/ie00082a018
- [5] Daher A, Chetouani Y, Hoblos G, Khalil M. Modified fuzzy c-means combined with neural network based fault diagnosis approach for a distillation column. IEEE Int Multidiscip Conf Eng Technol (IMCET). 2016;185-90. https://doi.org/10.1109/IMCET.2016.7777449
- [6] Orangi R, Mansourian H, Bina K, Rabbanifar S. Vulnerability assessment of steel structures in District 12 of Mashhad City and prioritizing the welding defects using the analytic hierarchy process. Int J Eng. 2018;31(6):877-85. https://doi.org/10.5829/ije.2018.31.06c.03
- [7] Berrekia H, Benzerg D, Haddi A. Behavior and damage of a pipe in the presence of a corrosion defect depth of 10% of its thickness and highlighting the weaknesses of the ASME/B31G method. Frat Integr Struct. 2019;13(49):643-54. https://doi.org/10.3221/IGF-ESIS.49.58
- [8] Belkacemi M, Benzerga D, Choutier A, Haddi A. Corroded Gas Pipeline Remaining Life Under Variable Pressure. **Iournal** UTeM. 2023 IMET 30:15(1):1-10. https://doi.org/10.54554/jmet.2023.15.01.001
- [9] Barrios AM, Burgos LM, Niebles-Nuñez EE, Espitia LA, Unfried-Silgado J. Influence of immersion corrosion on mechanical properties of AISI 430/AISI 316L dissimilar welded joints. Int J Eng Trans B Appl. 2021;34(5):1352-61. https://doi.org/10.5829/ije.2021.34.05b.31

- [10] Dobis JD, French DN. Damage mechanisms affecting fixed equipment in refining industry. Washington (DC): API Publishing Services; 2020.
- [11] Kang G, Luo H. Review on fatigue life prediction models of welded joint. Acta Mech Sin Xuebao. 2020;36(3):701-26. https://doi.org/10.1007/s10409-020-00957-0
- [12] Takahashi A, Toyohiro T, Segawa Y, Kobayashi M, Miura H. Embrittlement fracture behavior and mechanical properties in heat-affected zone of welded maraging steel. Materials (Basel). 2024;17(2). https://doi.org/10.3390/ma17020440
- [13] Ghassemi-Armaki H, Biro E, Sadagopan S. Advanced characterization of HAZ softening of AHSS for crash modeling. ISIJ Int. 2017;57(8):1451-60. doi:10.2355/isijinternational.ISIJINT-2016-649. https://doi.org/10.2355/isijinternational.ISIJINT-2016-649
- [14] Lemaitre J, Chaboche JL. Mechanics of solid materials. Shrivastava B, translator. Cambridge (UK): Cambridge University Press; 1990. https://doi.org/10.1017/CB09781139167970
- [15] Nekkaa B, Benzerga D, Haddi A. Damage analysis of corroded pipelines reinforced by composite materials. Int Rev Mech Eng. 2018;12(3):249-54. https://doi.org/10.15866/ireme.v12i3.13447
- [16] Mirmohammad SH, Safarabadi M, Karimpour M, Aliha MRM, Berto F. Study of composite fiber reinforcement of cracked thin-walled pressure vessels utilizing multi-scaling technique based on extended finite element method. Strength Mater. 2018;50(6):925-36. https://doi.org/10.1007/s11223-019-00041-4
- [17] Bilat A-S, Gourgues-Lorenzon A-F, Besson J, Richard G, Pineau A. Brittle fracture in heat-affected zones of girth welds of modern line pipe steel (X100). 2013.
- [18] El-taly BA, Abd El Hameed MF. The parameters effect on the structural performance of damaged steel box beam using Taguchi method. Int J Adv Struct Eng. 2018;10(1):1-15. https://doi.org/10.1007/s40091-018-0180-6
- [19] Messabih FZ, Bouchouicha B. Coupling between welding conditions and thermal cycling for identification of the mechanical heterogeneity of a weld joint. Period Polytech Mech Eng. 2018;62(3):226-32. https://doi.org/10.3311/PPme.12065
- [20] Lemaitre J, Lemaitre JA. Continuous damage mechanics model for ductile fracture. J Eng Mater Technol. 1985;107(1). https://doi.org/10.1115/1.3225775
- [21] Mehta V. Evaluation of the fracture parameters for SA-516 Grade 70 material. IOSR J Mech Civ Eng. 2016;13(3):38-45.
- [22] AWS. E7018/E7018-1 data sheet. 2008;713:9353-5.
- [23] Wang J, Baker A, Chang P. Hybrid approaches for aircraft primary structure repairs. Compos Struct. 2019;207:190-203. https://doi.org/10.1016/j.compstruct.2018.09.038
- [24] Baker A. Structural health monitoring of a bonded composite patch repair on a fatigue-cracked F-111C wing. Struct Health Monit. (n.d.).
- [25] Wu C, Zhao X, Duan W, Emdad MR, Al-Mahaidi R. Fatigue of center cracked steel plates with UHM CFRP plate strengthening. APFIS 2012 3rd Asia-Pacific Conf FRP Struct. 2012;15(10):1801-15. https://doi.org/10.1260/1369-4332.15.10.1801
- [26] Moreira RDF, de Moura MFSF, Silva FGA. Quasi-static and fatigue analyses of aluminium structures repaired by CFRP patch bonding. Compos Struct. 2023;322:117372. https://doi.org/10.1016/j.compstruct.2023.117372
- [27] Khayer Dastjerdi A, Tan E, Barthelat F. Direct measurement of the cohesive law of adhesives using a rigid double cantilever beam technique. Exp Mech. 2013;53(9):1763-72. https://doi.org/10.1007/s11340-013-9755-0
- [28] El Zghayar E, Mackie K, Xia J. Fiber reinforced polymer (FRP) composites in retrofitting of concrete structures: Polyurethane systems versus epoxy systems. Spec Publ. 2014;298:1-22.
- [29] Niu H, Wang S, Shen Y, Liu S, Jiang S, Qin T, Li T. Tough structural adhesives with ultra-resistance to both high and cryogenic temperature. Polymers (Basel). 2023;15(10). https://doi.org/10.3390/polym15102284
- [30] He P, Moreira Arouche M, Koetsier M, Pavlovic M. Mode I fracture behavior of glass fiber composite-steel bonded interface experiments and CZM. Compos Struct. 2024;330:110510. https://doi.org/10.1016/j.compstruct.2023.117814
- [31] Rodrigues VCMB, Marques EAS, Carbas RJC, Youngberg M, Dussaud A, Beygi R, da Silva LFM. The development and study of a new silylated polyurethane-based flexible adhesive-Part 2: Joint testing and numerical modelling. Materials (Basel). 2023;16(21). https://doi.org/10.3390/ma16217022
- [32] Benzerga D, Haddi A, Lavie A. Delamination model using damage mechanics applied to new composite for orthopaedic use. Int J Mater Eng. 2014;2014(3):103-13.
- [33] Lemaitre J. A course on damage mechanics. Berlin: Springer; 1992. https://doi.org/10.1007/978-3-662-02761-5
- [34] Suherman, Muliadi D, Ridho MS, Marpaung CP. Pengaruh kuat arus terhadap sifat mekanis dan struktur mikro. Ilm Mek. 2019;4(2):64-69.

- [35] Huang HH, Tsai WT, Lee JT. The influences of microstructure and composition on the electrochemical behavior of A516 steel weldment. Corros Sci. 1994;36(6):1027-38. https://doi.org/10.1016/0010-938X(94)90201-1
- [36] Patel S, Patel P, Mehta V. Experimental study of the effect of heat input on mechanical properties of TIG welded joints of SA516 grade 70 material. Int J Res Sci Innov. 2017;4(VS):29-35.
- [37] Amin AS, Hanna MS, Khider SA. Study of mechanical properties of carbon steel plate SA-516 Gr. 70 welded by SAW using V-shape joint design. Eng Technol J. 2020;38(2):152-65. https://doi.org/10.30684/eti.v38i2A.269
- [38] Yang Y. The effect of submerged arc welding parameters on the properties of pressure vessel and wind turbine tower steels. Saskatchewan: University of Saskatchewan; 2008.
- [39] Amanie J, Oguocha INA, Yang Y, Yannacopoulos S. The effect of welding speed on the impact and tensile properties of SA516 grade 70 steel. Saskatchewan: University of Saskatchewan; 2010.
- [40] Vercesi J, Surian E. The effect of welding parameters on high-strength SMAW all-weld-metal-part 2: AWS E10018-M and E12018-M. Weld J. 1998;77(4):164s-171s.
- [41] Luo J, Luo S, Li L, Zhang L, Wu G, Zhu L. Stress corrosion cracking behavior of X90 pipeline steel and its weld joint at different applied potentials in near-neutral solutions. Nat Gas Ind B. 2019;6(2):138-44. https://doi.org/10.1016/j.ngib.2018.08.002
- [42] Sharma SK, Maheshwari S. A review on welding of high strength oil and gas pipeline steels. J Nat Gas Sci Eng. 2017;38:203-17. https://doi.org/10.1016/j.jngse.2016.12.039
- [43] Lemaitre J, Doghri I. Damage 90: a post processor for crack initiation. Comput Methods Appl Mech Eng. 1994;115(3-4):197-232. https://doi.org/10.1016/0045-7825(94)90060-4
- [44] Bilat A-S. Estimation du risque de rupture fragile de soudures de pipelines en aciers à haut grade: caractérisation et modélisation. 2007.
- [45] Baghel PK. Effect of SMAW process parameters on similar and dissimilar metal welds: an overview. Heliyon. 2022;8(12):e12161. https://doi.org/10.1016/j.heliyon.2022.e12161
- [46] De Recherche D, De Recherche D. Modélisation hydrogéologique des aquifères de Paris et les écoulements souterrains. Paris: École Nationale Supérieure des Mines de Paris; 2013.
- [47] Benzerga D, Haddi A, Seddak A, Lavie A. A mixed-mode damage model for delamination growth applied to a new woven composite. Comput Mater Sci. 2008;41(4):515-21. https://doi.org/10.1016/j.commatsci.2007.05.022
- [48] Aljazaeri ZR, Al-Jaberi Z. Numerical study on flexural behavior of concrete beams strengthened with fiber reinforced cementitious matrix considering different concrete compressive strength and steel reinforcement ratio. Int J Eng Trans A Basics. 2021;34(4):796-802. https://doi.org/10.5829/ije.2021.34.04a.05
- [49] Hait P, Karthik R, Mitra R, Haldar R. Natural and artificial fibre reinforced concrete: a state-of-art review. Int J Eng Trans A Basics. 2024;37(3):503-10. https://doi.org/10.5829/IJE.2024.37.03C.07
- [50] Chouiter A, Benzerga D, Haddi A, Tamine T. Prediction of cycle life of expansion bellows for fixed tube sheet heat exchanger. Frat Ed Integrita Strutt. 2019;13(47):30-8. https://doi.org/10.3221/IGF-ESIS.47.03
- [51] Djahida D, Tewfik G, Witek M, Abdelghani M. Analytical model and numerical analysis of composite wrap system applied to steel pipeline. Materials (Basel). 2021;14(21):1-18. https://doi.org/10.3390/ma14216393